ACS OMEGA

Open Access

http://pubs.acs.org/journal/acsodf

Article

Reusable Magnetite Nanoparticle (Fe_3O_4 NP) Catalyst for Selective Oxidation of Alcohols under Microwave Irradiation

Francesca Pincella,* Katsuhiro Isozaki,* Ryota Sato, Toshiharu Teranishi, Hikaru Takaya,* and Masaharu Nakamura*

Cite This: *ACS Omega* 2024, 9, 24477−24488

Read Online

ACCESS | Metrics & More | Article Recommendations | Supporting Information

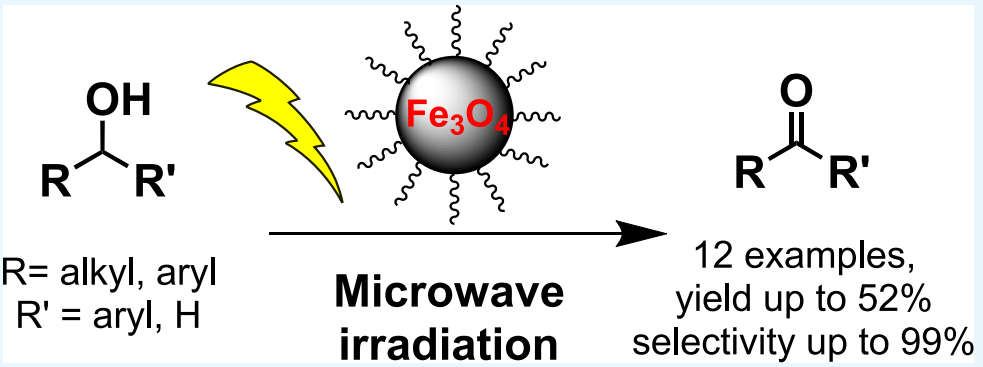

ABSTRACT: Iron oxide nanoparticles (NPs) are nontoxic and abundant materials which have long been investigated as reusable catalysts in oxidation reactions, but their use so far has been hampered by a low selectivity. Here, unsupported iron oxide NPs have been found to successfully catalyze the microwave-assisted oxidation of primary and secondary alcohols to their respective aldehydes and ketones with a high selectivity when *N*-methylmorpholine *N*-oxide was used as the terminal oxidant. The crystalline phase and size of the iron-based catalyst have a drastic effect on its activity, with small magnetite (Fe_3O_4) NPs being the optimal catalyst for this reaction. The nanocatalyst could be easily recovered by magnetoseparation and successfully recycled four times without any need for special pretreatment or reactivation step and with a minimal loss of activity. The subsequent loss of activity was attributed to the transition from magnetite (Fe_3O_4) to maghemite (γ-Fe_2O_3), as confirmed by X-ray diffraction, Fourier transform infrared, and X-ray absorption near-edge spectroscopy. The nanocatalyst could then be reactivated by the high-temperature microwave treatment and used again for the microwave-assisted oxidation reaction.

INTRODUCTION

Iron oxide nanoparticles (NPs) have attracted increasing attention for their applications as nontoxic, easily recoverable, recyclable, and earth-abundant-metal catalysts, a promising affordable alternative to traditional noble metal catalysts.[1−4] Iron oxide NPs are amenable not only to magnetic separation[5] but also to microwave (MW) activation,[6] thanks to their superparamagnetic properties which spur their practical applications in synthetic organic reactions.[7−13] Oxidation reactions, in particular, are of great importance for the chemical industry, representing the second most utilized chemical process after polymerization.[14−18] Typically, among heterogeneous catalysts, supported or dual catalysts have been the main focus of the research toward the development of new and sustainable liquid-phase alcohol oxidation reactions, with iron oxides used either as a magnetic support for other metal or organic catalysts to improve recovery and recycling or as active catalysts supported on porous matrices.[19,20] When iron oxide, alumina, silica, or carbon-based materials are used as supports, though, the catalytic activity of the main active species is often found to be influenced by the support, and a synergistic effect is anticipated.[21−25] The complex synthesis of these supported catalysts and the interplay of the various active species, therefore, make the characterization and optimization of these heterogeneous catalysts very challenging.

Many reports have also described the ability of various unsupported iron oxide NPs to catalyze oxidation or mineralization reactions in the presence of a stoichiometric terminal oxidant (most notably hydrogen peroxide).[26−33] Despite the many advantages of a system consisting of a simple iron-based catalyst and a green oxidant such as

Received: January 11, 2024
Revised: April 16, 2024
Accepted: April 22, 2024
Published: May 29, 2024

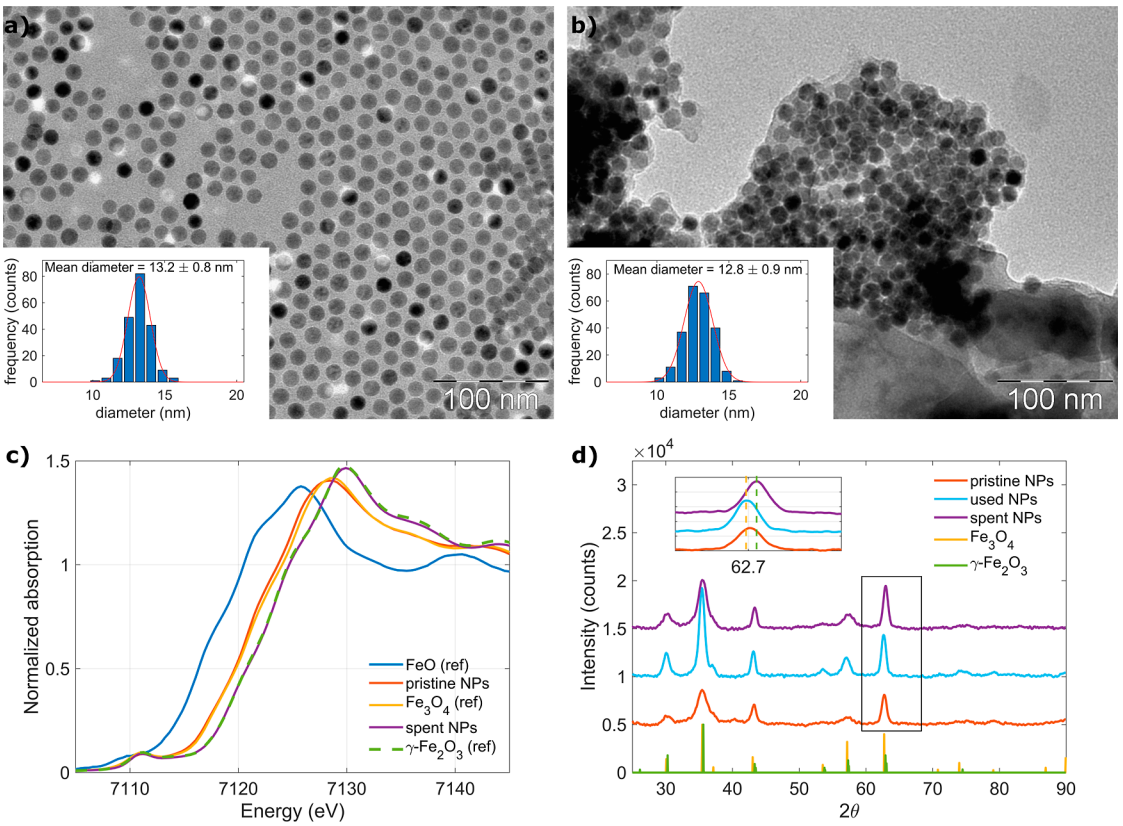

Figure 1. (a) TEM image of pristine stearate-capped magnetite NPs. Inset: size distribution of the NPs. The mean diameter is 13.2 ± 0.8 nm. (b) TEM image of once-used iron oxide NPs. Inset: size distribution of the NPs. The size is 12.8 ± 0.9 nm. The NP aggregation on the TEM grid is due to the removal of the stearate ligand. (c) Fe K-edge XANES spectra of pristine (red line) and spent (purple line) iron oxide NPs and reference spectra of FeO (wüstite, blue), Fe_3O_4 (magnetite, yellow), and γ-Fe_2O_3 (maghemite, green). The spectrum of the pristine NPs almost perfectly overlaps with that of magnetite, while that of spent NPs overlaps with that of maghemite. (d) XRD spectra of pristine (red line), once-used (light blue), and spent (purple line) iron oxide NPs and the reference powder diffraction peaks from magnetite (yellow line) and maghemite (green line). Inset: a clear 440 peak shift for the spent catalyst can be observed, which can be attributed to the phase change.

hydrogen peroxide, the main drawback for these oxidation reactions is their low selectivity associated with their tendency to form overoxidation products via a Fenton reaction.[34−37] Fenton (or photo-Fenton) reactions with iron oxide nanocatalysts have often been proposed for advanced oxidation processes in the treatment of wastewater since trace organic pollutants can be fully oxidized to harmless compounds, i.e., water and carbon dioxide.[29,38−40] This catalytic system benefits from its simplicity and low cost, but the lack of selectivity has limited its applications in industrial settings. To the best of our knowledge, two previous reports by Beller et al. have been so far the most notable examples of methods taking advantage of unsupported iron oxide nanocatalysts for primary and secondary alcohol oxidation in the presence of hydrogen peroxide as an oxidant.[30,33] The aforementioned catalytic systems afforded the target oxidation products in low to medium yields and with a medium to good selectivity. For the aforestated reasons, a new simple, selective, and cost-effective method that combines the beneficial characteristics of the iron oxide nanocatalyst with the high selectivity of conventional oxidation methods is urgently needed.[41]

In this study, we have developed a new selective oxidation of primary and secondary alcohols catalyzed by unsupported iron oxide NPs, specifically magnetite nanoparticles (Fe_3O_4 NPs) under MW irradiation. Target aldehydes and ketones are produced in a medium yield with a high selectivity by adding *N*-methylmorpholine *N*-oxide (NMO) as a terminal oxidant, which is also employed as a commodity chemical by the pulping industry.[42−47] Furthermore, we have verified the catalytic activity of various unsupported iron-based heterogeneous catalysts with different chemical compositions [Fe(II) to Fe(III) ratio], crystalline phase, and size. Among the iron oxide species tested, only magnetite was found to be catalytically active, and the smallest magnetite nanoparticles, 13 nm Fe_3O_4 NPs, showed the best catalytic performance, in line with typical considerations regarding the importance of the available surface area. The chemical and morphological characteristics of the recyclable catalyst have also been characterized by various analytical techniques before and after several catalytic cycles. The unsupported Fe_3O_4 NPs catalyst showed no morphological or chemical changes except ligand detachment after use and could be recycled 4 times with no loss in activity. Deactivation of the catalyst, corresponding to the oxidation to a catalytically inactive Fe(III)-rich maghemite phase (γ-Fe_2O_3), occurred after multiple uses. These findings demonstrated that for this catalytic system, the chemical composition was the most important parameter, followed by the size of the iron oxide NPs.

RESULTS AND DISCUSSION

Iron Oxide Characterization. Iron oxide NPs were characterized by transmission electron microscopy (TEM) to ascertain their morphology and size (Figures 1 and S1 in Supporting Information). The average diameter of the pristine

https://doi.org/10.1021/acsomega.4c00361
ACS Omega 2024, 9, 24477−24488

C_{18}-Fe_3O_4 NPs is 13.2 ± 0.8 nm, with a very narrow size distribution. The details of all the catalysts used are summarized in Table 1. With the pristine catalyst, we refer to the NPs before use; with the used catalyst, we refer to NPs that have been used for one reaction cycle and are still catalytically active; and with the spent catalyst, we refer to NPs which have been confirmed to be no longer catalytically active and have been collected after repeated oxidation cycles. The spent catalyst maintains the spherical shape of the pristine NPs, while its color changes from black to red (see Figure S1a) and the size (diameter 14 ± 1 nm) slightly increases. We should point out that the aggregation of the spent catalyst is due to the complete detachment of the stearate ligand from the NP surface, as confirmed also from Fourier transform infrared (FT-IR) spectra (Figure 2). The slight increase in size can be explained by the formation of a FeOH layer at the surface of the NPs, which is also compatible with the increased hydrophilicity of the spent NPs and with the presence of broad OH vibrations at 1050 and 1630 cm^{-1} in the FT-IR spectrum.[33,48−51]

Table 1. List of Heterogenous Catalysts with Their Respective Size

entry	catalyst	size (nm)
1	C_{18}-Fe_3O_4	13.2 ± 0.8
2	Fe_3O_4	50−100[a]
3	γ-Fe_2O_3	<50[a]
4	FeO	<2 × 10[6][a]
5	C_{18}-Fe_3O_4 used 1 time	12.8 ± 0.9
6	Spent C_{18}-Fe_3O_4	14 ± 1

[a]As declared by the manufacturer.

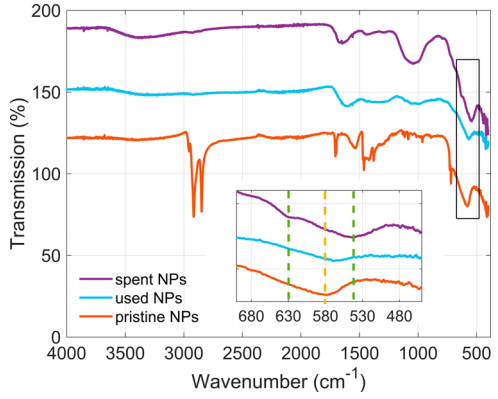

Figure 2. From the top: IR spectra of spent iron oxide NPs, used iron oxide NPs, and pristine iron oxide NPs. Inset: Fe−O vibration region. The original peak for pristine magnetite particles (yellow dotted line at 580 cm^{-1}) is clearly found to shift to lower wavenumbers and split into two peaks when the catalyst is deactivated (green dotted lines at 544 and 630 cm^{-1}).

The crystalline phase of the pristine NPs was confirmed by X-ray diffraction (XRD), X-ray absorption near-edge spectroscopy (XANES), and FT-IR (Figure 1). From XANES, it was possible to compare the spectrum of the pristine and spent C_{18}-Fe_3O_4 NPs with the reference spectra of Fe_3O_4, γ-Fe_2O_3, and FeO (Figure 1c). The pristine spectrum C_{18}-Fe_3O_4 NPs overlapped almost completely with that of the reference Fe_3O_4, confirming that the as-synthesized particles are magnetite particles.[52] The spectra were processed and analyzed with Athena (IFEFFIT package) by a linear combination fit using the spectra of the reference iron compounds as standards. It was found that the pristine C_{18}-Fe_3O_4 NPs are mostly magnetite (94.3% Fe_3O_4) with a small contribution from wüstite Fe(II)O (5.7% FeO) (Figures 1 and S2), as discussed in a previous report.[53] The XANES spectrum of spent C_{18}-Fe_3O_4 NPs instead corresponds to that of γ-Fe_2O_3 (Figures 1 and S2).

The pristine C_{18}-Fe_3O_4 NP composition was confirmed by elemental analysis and thermogravimetric and differential thermal analysis (TG-DTA); see Figure S3. It was found that the ligand corresponds to approximately 20 wt % of the capped NPs (this value oscillates slightly based on the sample batch), which translates to a stearate surface density of 6 × 10^{14} molecules/cm^2.

From the analysis of the XRD spectra in Figure 1, it can be concluded that C_{18}-Fe_3O_4 NPs are magnetite NPs, with a diameter of 13 nm according to Debye−Scherrer analysis. No remarkable change in the XRD spectrum can be observed for once-used NPs. The only difference in the spectrum of once-used particles is in the slight narrowing of the diffraction peaks, suggesting a larger crystalline size, which can be explained by the removal of defects due to either heating or ligand removal. The positions of the diffraction peaks and relative fwhm for all samples are reported in Table S1. The spectrum of the spent catalyst, instead, shows a small shift of the 440 peak from 62.7 to 62.9° (see the inset in Figure 1) and a decrease in the relative intensity of the smaller peaks at higher scattering angles, compatible with a γ-Fe_2O_3 phase, as determined by XANES. It is therefore suggested that pristine Fe_3O_4 NPs undergo a change in the crystalline phase to give catalytically inactive maghemite nanoparticles after several uses.

The transformation from magnetite to maghemite was also confirmed by FT-IR spectroscopy.[54,55] In Figure 2, we can notice the FT-IR spectra of pristine, once-used, and spent NPs. At first, we can notice that all C−H and COO^- stretching vibrations that originate from the ligand molecules can be clearly observed for pristine particles but are not detected for the once-used and spent catalyst NPs [see Figure S4 for stearic acid and Fe(III)-stearate FT-IR spectra]. The FT-IR spectrum of spent NPs shows broad peaks at 1050, 1420, 1630, and 3400 cm^{-1}. These peaks probably originate from terminal OH groups and loosely bound water on the NP surface.[56−58] From Figure 2 and Table S2, we can also notice that the position of the frequency of the Fe−O vibration for once-used NPs (569 cm^{-1}) corresponds to the expected value for magnetite; the slightly higher frequency for fresh NPs can be due to a strain in the Fe−O bond induced by the ligand. The Fe−O peak for spent NPs is split, the frequency of the main peak is shifted to 544 cm^{-1}, and a smaller peak appears at 630 cm^{-1}. This behavior is compatible with the phase change from Fe_3O_4 to γ-Fe_2O_3.[55,59−62]

Oxidant Screening. Various oxidants have been tested for the oxidation reaction with 1-phenylethanol **1** as the starting material and C_{18}-Fe_3O_4 NP as the catalyst (Table 2). The secondary benzylic alcohol 1-phenylethanol was chosen as the model substrate for reaction optimization. The use of hydrogen peroxide as the oxidant, the most common oxidant for iron oxide-based oxidation reactions, resulted in a low yield and low selectivity, unlike previous reports using different types of iron oxide catalysts,[24,30] but, most importantly, the iron oxide NPs were transformed into a red slurry which is difficult

https://doi.org/10.1021/acsomega.4c00361
ACS Omega 2024, 9, 24477−24488

Table 2. Oxidant Screening[a]

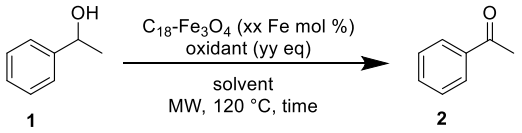

entry	xx (Fe mol %)	oxidant (eq)	solvent	time (h)	yield[b] (%)	RSM (%)	selectivity (%)
1	4		MeCN	15	0.8	98	40
2	4	H_2O_2 (3)	MeCN/H_2O (9:2 v/v)	5	5	88	42
3	4	*m*-CPBA (1)	MeCN	15	43	18	52
4	0	*m*-CPBA (1)	MeCN	15	41	5	43
5	4	$PhI(OAc)_2$ (1)	MeCN	5	41	22	53
6	4	periodic acid (1)	MeCN	5	0.8	73	30
7	4	O_2 (1 atm)	MeCN	5	0.8	99	80
8	4	oxone (1)	MeCN	5	6	80	30
9	4	NMO (1)	MeCN	15	33	67	>99
10	4	TMANO (1)	MeCN	15	2	98	>99
11	4	PNO (1)	MeCN	15	1	99	>99

[a]General reaction conditions: 0.8 mmol of **1**, 3.2 mg of catalyst, 0.8 mmol (1 equiv) or 2.4 mmol (3 equiv) of oxidant, 0.8 mL of solvent in a MW sealed tube under constant stirring, and MW reactor in a fixed temperature mode (MW power is automatically adjusted to keep T = 120 °C). TMANO = trimethylamine *N*-oxide; PNO = pyridine *N*-oxide; RSM = recovered starting material (1); selectivity (%) = yield (%) of **2**/(100 − conversion). [b]The yield is calculated by ^{1}H NMR using 1,1,2,2-tetrachloroethane as an internal standard.

to separate and impossible to recycle. A similar fate befell to the NP catalysts when *m*-chloroperbenzoic acid (*m*-CPBA) was used as the oxidant. Furthermore, *m*-CPBA was found to oxidize the substrate even in the absence of the catalyst with a similar yield. The low mass balance of the oxidation reactions in the presence of *m*-CPBA suggests that overoxidation occurs. The reaction in the presence of (diacetoxyiodo)benzene [$PhI(OAc)_2$], entry 5 in Table 2, instead gave a 41% yield of acetophenone **2**, in addition to a mixture of unidentified products. Other oxidants, such as periodic acid, molecular oxygen, and oxone, did not afford any relevant amount of the target product **2**. NMO, instead, was found to afford **2** in a medium 33% yield with an excellent selectivity. Nevertheless, the oxidation reaction did not proceed in the presence of different *N*-oxides such as trimethylamine *N*-oxide (TMANO) and pyridine *N*-oxide (Table 2, entries 10 and 11).

Catalyst Screening. In addition to the stearate-capped NPs C_{18}-Fe_3O_4, various iron-based NP catalysts were tested for the oxidation reaction of 1-phenylethanol **1**, namely, γ-Fe_2O_3, FeO, and Fe_3O_4 (Table 3).

We can notice that C_{18}-Fe_3O_4 NP gives the highest yield of **2** in 46%, while the product in the absence of a catalyst is only 5% (entry 5). The synthesized catalyst C_{18}-Fe_3O_4 NP is remarkably more active than that of commercially available Fe_3O_4 (entry 2). The lower catalytic performance of commercially available magnetite is likely due to the larger radius (50−100 nm according to the manufacturer) of the NPs, which would correspond to a lower surface to volume ratio and therefore limited availability of catalytically active sites on the larger NP surface. The other two iron oxides tested, γ-Fe_2O_3 and FeO, did not catalyze the oxidation reaction (entries 3 and 4), suggesting the importance of the presence of both Fe(II) and Fe(III) species on the catalyst surface. In conclusion, the composition of the iron nanocatalyst can be described as the main factor controlling its catalytic activity, with the surface area also being an important parameter for the optimization of the catalyst.

From Table S3, we can also analyze the effect of catalyst loading on the yield of target product **2** and on the catalyst turnover number (TON) and frequency (TOF). From Table S3, we can notice that the TON increases for increasing iron loading up to a loading of 4 Fe mol %, from a TON of 2.3 for 1.3 Fe mol % to a TON of 8.3 for 4 Fe mol %, and then decreases for loadings higher than 4 Fe mol %. We have therefore determined that the optimal catalyst loading is 4 Fe mol % corresponding to 3.2 mg of C_{18}-Fe_3O_4 NP in standard reaction conditions. This nonmonotonous tendency can be due to the role of the catalyst in the autocatalytic degradation of NMO to *N*-(methylene)morpholinium ions and *N*-formylmorpholine, which is known to be induced by the presence of redox−active transition metals, especially at temperatures above 100 °C.[47] While the increase in catalyst loading results in a higher catalytic activity toward both the oxidation of **1** and the autocatalytic NMO degradation, the second one likely dominates at high catalyst loadings, limiting the availability of the terminal oxidant for catalyst regeneration and therefore also the final yield of the target product.

Table 3. Catalyst Screening[a]

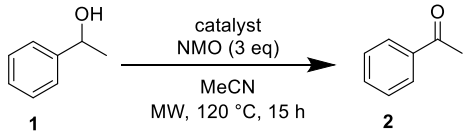

entry	catalyst (Fe mol %)[b]	yield[c] (%)	RSM (%)	TON[d]	TOF[e] (h^{-1})
1	C_{18}-Fe_3O_4 (4)	46	54	11.5	0.77
2	Fe_3O_4 (4)	21	79	5.3	0.35
3	γ-Fe_2O_3 (4)	3	97	0.8	0.053
4	FeO (4)	2	98	0.5	0.033
5	no catalyst (0)	5	94	n.a	n.a

[a]General reaction conditions: 0.8 mmol of **1**, 2.4 mmol (3 equiv) of NMO, 0.8 mL of acetonitrile in a MW sealed tube under constant stirring, and an MW reactor in a fixed temperature mode (MW power is automatically adjusted to keep T = 120 °C). n.a.: not available. [b]The catalyst loading is calculated from (moles of Fe atoms)/(moles of **1**) × 100. [c]The yield is calculated by ^{1}H NMR using 1,1,2,2-tetrachloroethane as an internal standard. [d]TON: (number of moles of **2**)/(Fe mol of catalyst). [e]TOF: (number of moles of **2**)/[(Fe mol of catalyst) × time].

https://doi.org/10.1021/acsomega.4c00361
ACS Omega 2024, 9, 24477−24488

Optimization of Reaction Conditions: Oxidant Loading, Temperature, Solvent, Concentration, Support, and Heating Source. The effect of different oxidant loadings was tested at first, and it was found that the yield increases slightly with higher NMO loading as shown in Table S4, and therefore, an optimal loading of 3 equiv of NMO was typically used (higher oxidant loadings were considered unsuitable for both environmental and economic reasons), except for mechanistic studies where 1 equiv of NMO was preferred. The effect of temperature on the MW-assisted reaction was also investigated. When 1 equiv of NMO was used, it was found that an increase in temperature resulted in a higher reaction yield up to 100 °C (Table S5). The yield was almost constant for a temperature of 120 °C but then decreased for a temperature of 140 °C (Table S5, entries 2 and 3). When the amount of the terminal oxidant was set to 3 equiv, we could notice that the highest yield was achieved for the reaction at 120 °C (Table 4, entry 2) compared to either lower or higher reaction temperatures (Table 4, entries 1 and 3). These results suggest that the temperature affects not only the target oxidation reaction but also the autocatalytic degradation of NMO, as previously mentioned. In all reactions, regardless of the final yield of the target compound, NMO was fully consumed.

Table 4. Optimization of Reaction Temperature[a]

entry	temperature (°C)	yield[b] (%)	RSM[b] (%)
1	100	32	68
2	120	46	54
3	150	28	72

[a]General reaction conditions: 0.8 mmol of 1-phenyl ethanol, 3.2 mg of C_{18}-Fe_3O_4 catalyst (corresponding to 4 Fe mol %), 2.4 mmol (3 equiv) of NMO, 0.8 mL of acetonitrile in a MW sealed tube under constant stirring, and an MW reactor in a fixed temperature mode for 15 h (MW power is automatically adjusted to maintain the target temperature). [b]Yield is calculated as an ^{1}H NMR yield using 1,1,2,2-tetrachloroethane as an internal standard.

In addition to the reaction temperature optimization, we have also performed the solvent screening to determine the best solvent, and we have concluded that acetonitrile provided the best performance (Table S6). Concerning the substrate concentration, the highest yield was obtained when the substrate was present in 1 M concentration (Table S7). It was also confirmed that the catalyst performs better as a free catalyst, without the need to be loaded onto a solid support such as porous silica−alumina (Figure S5, Table S8), showing a remarkable advantage compared to the most common iron-oxide-based oxidation catalysts. Finally, apart from its known superior energy efficiency and higher heating rates,[63] the main advantage of using MW heating in this oxidation reaction was the possibility to perform the oxidation reaction in a low-molecular-weight solvent (acetonitrile) at a temperature above its boiling point (Table S9), which was not accessible to standard heating. We have also compared standard and MW heating with the same reaction mixture using a similar solvent, hexanenitrile, whose boiling point is above 120 °C (Table S9, entries 3−4). The yield for the MW-assisted reaction (35%) was slightly lower than that for the standard heating reaction (46%); while in both cases, the catalyst was not fully recovered after the reaction, and the standard heating reaction resulted in a more extensive dissolution of the catalyst (red slurry) compared to that of the MW-assisted reaction in hexanenitrile. This difference might be related to the ability of iron oxide NPs to absorb MW irradiation and to generate highly localized heat.[64] The complete dissolution of the NPs with standard heating, furthermore, eliminates the main advantage of magnetic NPs that is their easy separation and recyclability.

Substrate Scope. A series of benzylic and allylic primary and secondary alcohols were screened for the MW-assisted oxidation reaction in the presence of C_{18}-Fe_3O_4 NP as the catalyst and NMO as the terminal oxidant (Table 5). The reaction time was adjusted to 30 min for primary alcohols due to their higher reaction rate and higher susceptibility to overoxidation. Furthermore, acetonitrile was replaced by deuterated acetonitrile, and the reaction progress was evaluated by collecting small aliquots of the reaction mixture to be analyzed by quantitative ^{1}H NMR. The catalyst was found to promote the oxidation of secondary benzylic alcohols with a medium yield and an excellent selectivity (Table 5, entries 1−6), of secondary allylic alcohol (Table 5, entry 7) with a medium yield and selectivity, and of primary benzylic alcohols with a medium yield and good selectivity (Table 5, entries 8 and 9). Benzhydrol was efficiently oxidized to benzophenone in a 52% yield with a complete selectivity (entry 1). Both secondary benzylic alcohols bearing electron-donating and electron-withdrawing substituents participate in this reaction, giving moderate yields (entries 2−5). Sterically hindered ortho-substituent and a coordinative heteroaromatic ring resulted in lower yields of the corresponding ketone products (entries 4 and 6). Secondary cyclic alcohol, cyclohexanol, gave a 16% yield of cyclohexanone with a lower selectivity (entry 7). The catalyst also promoted the oxidation of a variety of primary allylic alcohols, such as benzylic alcohol, and also primary alkyl alcohols in a low to moderate yield (entries 8−11). Benzaldehyde was selectively obtained in 36% yield from the oxidation of benzyl alcohol without the formation of an overoxidation product of benzoic acid (entry 8). Cinnamic alcohol was converted to cinnamaldehyde in 34% yield with little side products (entry 9). Octanol was also oxidized to octanal in 12% yield (entry 10) and 2,2-dimethylpropane-1,3-diol gave the monoaldehyde 3-hydroxy-2,2-dimethylpropanal as the main product in 6% yield (entry 11). Considering the apparent reaction rates, the reaction rate decreases in the following order: primary benzylic alcohols, secondary benzylic alcohols, primary aliphatic alcohol, and finally secondary aliphatic alcohols.

Catalyst Recycling. The main advantage of using unsupported Fe_3O_4 NPs as a catalyst is their recyclability and simple magnetoseparation from the reaction mixture (Figure S6). To verify the recyclability of the C_{18}-Fe_3O_4 NP, the catalyst was removed from the reaction mixture by magnetoseparation, rinsed three times with acetonitrile, and dried in air before reuse. No further treatment, such as annealing, was applied to the used catalyst. A batch of once-used catalyst was also characterized by TEM, XRD, and FT-IR (Figures 1 and 2). From the characterization of the used catalyst (Figures 1 and 2), we could conclude that the ligand (stearate) was almost completely removed from the catalyst surface after one use; only weak residual CH_2 and CH_3 IR peaks can be observed at 2850 and 2915 cm^{-1} (Table S2).

New broad IR bands centered around 990−1050 and 1610−1650 cm^{-1} appeared in the FT-IR spectra of the once-used and spent NPs. These bands can be attributed to OH vibrations and loosely bound water on the surface of the NPs.[65] The

https://doi.org/10.1021/acsomega.4c00361
ACS Omega 2024, 9, 24477−24488

Table 5. Substrate Scope[a]

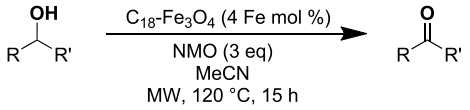

entry	substrate	product	conversion (%)	selectivity (%)	TON[d]	TOF[e] (h^{-1})
1	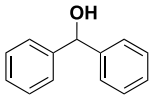	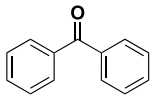	52	>99	13	0.87
2	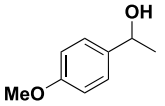	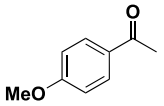	48	>99	12	0.80
3	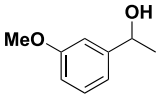	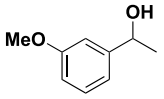	45	99	11.3	0.75
4	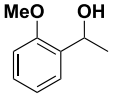	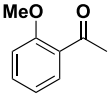	27	>99	6.8	0.45
5	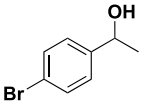	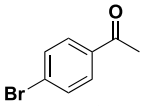	44	91	10	0.67
6	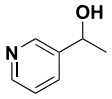	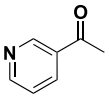	23	>99	5.8	0.39
7[b]			16	57	3.9	0.26
8[c]			36	>99	27	54
9[c]	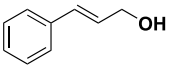	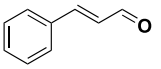	34	72	8.5	17
10[c]	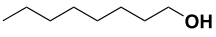	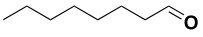	12	39[f]	3.0	6.0
11[c]			6	83	1.3	2.6

[a]General reaction conditions: 0.8 mmol of primary or secondary alcohol, 3.2 mg of catalyst, 2.4 mmol (3 equiv) of NMO, 0.8 mL of acetonitrile in an MW sealed tube under constant stirring, and an MW reactor in a fixed temperature mode (MW power is automatically adjusted to maintain T = 120 °C). [b]Yield and recovered starting material were calculated by gas chromatography (GC) with dodecane as an internal standard. [c]The reaction time is 30 min in MeCN-d_3. Yield is calculated by ^{1}H NMR using 1,3,5-trimethoxybenzene as an internal standard. [d]TON: (number of moles of target product)/(Fe mol of catalyst). [e]TOF: (number of moles of target product)/[(Fe mol of catalyst) × time]. [f]Recovered starting material was calculated by GC with dibutyl ether as an internal standard.

broad peak centered around 3400 cm^{-1} also becomes more prominent with use, indicating the increased presence of OH groups on the catalyst surface. This different surface structure was also evident from the different dispersibility of the used particles; while the pristine particles are dispersible in hexane and toluene, the used and spent NPs are mildly dispersible in alcohols and not in hexane or toluene. From the XRD spectrum and the frequency of the Fe−O vibration in the FT-IR spectrum, it is evident that the crystalline phase of the NPs is not remarkably altered after the catalyst is used once.

The once-used catalyst was added to 0.8 mmol of 1-phenylethanol **1**, 0.8 mL of acetonitrile, and 2.4 mmol of NMO, and the MW-assisted reaction was performed according to the standard reaction conditions. As a result, it was found that the Fe_3O_4 NPs were still active and that the reaction yield was approximately the same as for the first use (Table 6, entries 1 and 2). This result confirms that the surface capping molecule does not play any role in the oxidation reaction, as discussed in the Supporting Information. A C_{18}-Fe_3O_4 catalyst was then reused multiple times (Table 6, entries 3−7), and it was found that approximately the same yield was observed for the first 4 cycles, while a 33% decrease in the target product was observed in the fifth cycle. To understand the reason for the inactivation of the catalyst, we have characterized a batch of fully inactivated catalyst (spent catalyst), and we concluded that the catalyst inactivation was linked to the phase transition from magnetite Fe_3O_4 to maghemite γ-Fe_2O_3. As shown in Figure 1, for a fully inactivated catalyst, in fact, the XRD

https://doi.org/10.1021/acsomega.4c00361
ACS Omega 2024, 9, 24477−24488

Table 6. Catalyst Recyclability[a]

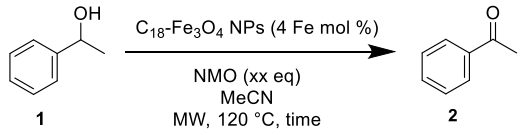

entry	cycle	NMO (eq)	time (h)	yield (%)	RSM (%)
1	1	3	15	43[b]	57[b]
2	2	3	15	40[b]	60[b]
3	1	1	5	27[c]	73[c]
4	2	1	5	27[c]	73[c]
5	3	1	5	27[c]	73[c]
6	4	1	5	25[c]	75[c]
7	5	1	5	18[c]	82[c]

[a]General reaction conditions: 0.8 mmol of **1**, 3.2 mg of C_{18}-Fe_3O_4 catalyst, 0.8 mmol (1 equiv) or 2.4 mmol (3 equiv) of NMO, 0.8 mL of acetonitrile in an MW sealed tube under constant stirring, and an MW reactor in a fixed temperature mode (MW power is automatically adjusted to maintain T = 120 °C). [b]Yield is calculated by ^{1}H NMR using 1,1,2,2-tetrachloroethane as an internal standard. [c]Yield is calculated by ^{1}H NMR using 1,3,5-trimethoxybenzene as an internal standard.

spectrum and the FT-IR spectrum showed a shift in the diffraction and vibrational peaks compatible with the presence of γ-Fe_2O_3. This result, together with the result in Table 3, entry 9, where commercially available γ-Fe_2O_3 NPs (size < 50 nm) were used, confirms that γ-Fe_2O_3 NPs, regardless of size, are not catalytically active for this oxidation reaction and that the presence of Fe(II) species is therefore indispensable.

With the deactivation of the catalyst linked to its transition from magnetite to maghemite, we have also demonstrated that the catalyst could be regenerated and the yield fully recovered to its initial state after one reaction cycle at high temperature (see Supporting Information).

Time-Course Study. Once it was clarified that the catalyst itself is not permanently deactivated during a single reaction cycle, we investigated the reason why the catalytic reaction stops before the full conversion of the starting material. Thus, we performed a time-course study to understand the fate of the oxidant (NMO) and catalyst during one reaction cycle for both pristine and used catalysts. The oxidation reaction was found to be a zero order with respect to NMO (see Figure S8) and a first order with respect to the reactant **1**, with the reaction rate more than 1.5 times faster for the used NP catalyst than that for pristine ones, as shown in the inset in Figure 3. The latter result also suggests that the presence of surface capping molecules has a negligible effect on this reaction, with once-used bare NPs only providing a moderately higher initial reaction rate compared to that of stearate-capped NPs. The yield of the target compound then reached the same plateau value, irrespective of the NPs used. In fact, the final reaction yield is not affected by the surface capping molecule, as previously discussed. We can also conclude that in both cases, the reaction is completed in about 1 h. Based on these results, we can calculate the effective TOF for the pristine and used NP catalyst from the 30 and 60 min data point: the TOF values for the pristine NPs are 7.3 h^{-1} (30 min point) and 6.4 h^{-1} (60 min point), while for the used NPs, the TOF values are 10.5 h^{-1} (30 min point) and 6.8 h^{-1} (60 min point).

In the time-course study (Figure S8), in the first 30 min of the reaction, 2 equiv of NMO are consumed for each equivalent of the starting material that is oxidized. The data

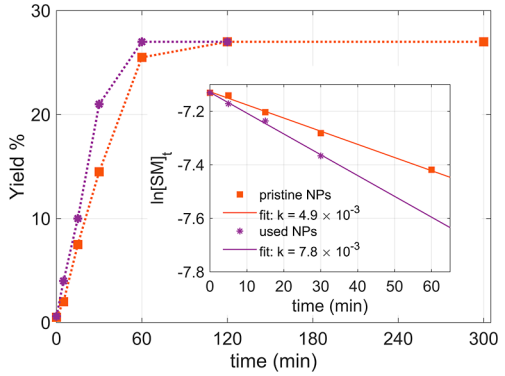

Figure 3. Time-course study performed with pristine stearate-capped iron oxide NPs (red squares and red dotted line) and once-used (bare) iron oxide NPs (purple stars and purple dotted line). Inset: decay profiles for first-order reactions with pristine (red) and once-used (purple) catalysts. The solid lines represent the linear fit of the natural logarithm of the concentration of the starting material versus time. The reaction rate coefficient k of once-used NPs is found to be 1.6 times higher than that of pristine NPs. Standard reaction conditions: 0.8 mmol of 1-phenyl ethanol, 0.8 mmol (1 equiv) of NMO, 4 Fe mol % of iron oxide catalyst (pristine NPs or once-used NPs), 0.8 mL of acetonitrile in an MW sealed tube under constant stirring, and an MW reactor in a fixed temperature mode (MW power is automatically adjusted to keep T = 120 °C).

in Figure S8 also indicate that NMO is not fully converted to *N*-methylmorpholine (NMM), which is its reduced form. The background degradation of NMO in the presence of the catalyst was confirmed by the time-course trace of NMO (Figure S9). This phenomenon is considered to be the well-known autocatalytic degradation of NMO to morpholinium ions and *N*-formylmorpholine, as described earlier.[47,66,67] From the time course (Figure S8), it is clear that the oxidation reaction stops when the concentration of NMM is larger than that of NMO, shifting the reaction equilibrium to the outside of the catalytic cycle (see Scheme 1). Therefore, we can conclude that the autocatalytic degradation of NMO is responsible for the early inhibition of catalyst turnover during the oxidation reaction. The autocatalytic degradation of NMO and presence of excess NMM, though, do not permanently deactivate the catalyst, which can in fact be recycled after use but only limit the catalyst turnover and final yield of the target product during a single reaction.

Proposed Catalytic Cycle. Based on the results shown earlier, we have proposed the following catalytic cycle (Scheme 1). It is to be noted that this catalytic cycle would not be sustained with either wüstite or maghemite as catalytic species; the presence of both Fe(II) and Fe(III) is necessary for this catalytic reaction. The as-prepared C_{18}-Fe_3O_4 NP **A** has both Fe(II) and Fe(III) sites on the surface covered by stearate ligands. The first step of oxidation (catalyst activation) of **A** with NMO is considered to afford catalytic active species **B** which oxidizes alcohols to give aldehyde/ketone products, together with the formation of the hydrogenated intermediate **C** by detachment of stearic acid, as confirmed by the IR spectrum of the recovered catalyst (Figure 2). Similar to the original catalyst, the catalyst **C** was also oxidized by NMO to afford the catalytic active species **D** which facilitates the efficient oxidation of alcohols into aldehyde/ketone products in a higher reaction rate than that of the original catalyst, as observed in the time-course study (Figure 3). The surface bridging hydroxy group of intermediate **D** is exchanged by the

https://doi.org/10.1021/acsomega.4c00361
ACS Omega 2024, 9, 24477−24488

Scheme 1. Proposed Catalytic Cycle

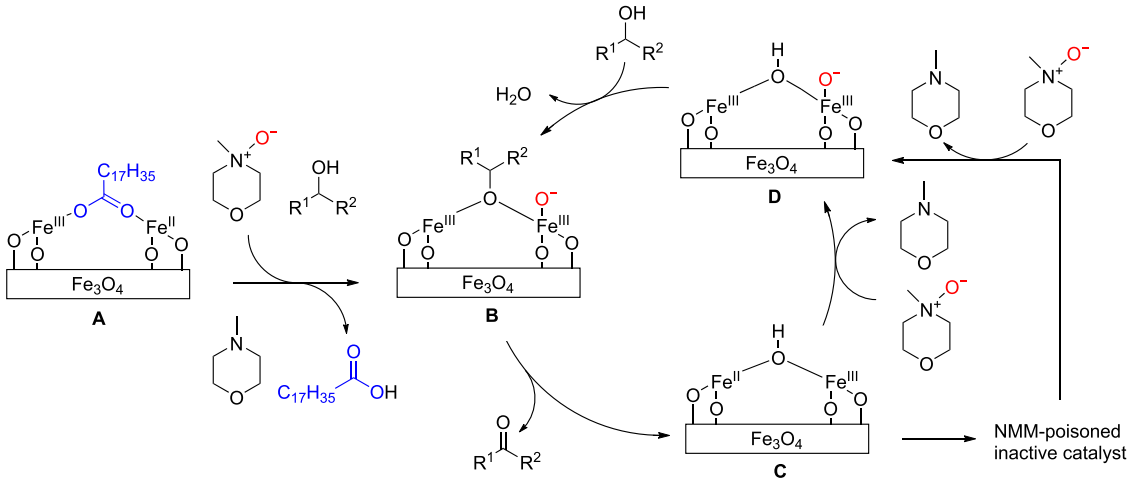

alcohol substrate to form the alkoxide-bridged intermediate **B**. The smooth deprotonation of the alpha-proton of the bridging alkoxide takes place to detach the aldehyde/ketone product and regenerate the hydroxylated Fe_3O_4 **C**. As evidenced by the time-course studies (Figures 3, S8, and S9), in situ-generated NMM acts as a catalyst poison inactivating the catalyst. The addition of NMO enables the catalyst to be regenerated in recycled catalytic reactions (Table 6).

CONCLUSIONS

In conclusion, it was found that Fe_3O_4 NPs can catalyze the MW-assisted oxidation reaction of primary and secondary benzylic and aliphatic alcohols to aldehydes and ketones, respectively, in the presence of NMO as a terminal oxidant with a medium yield and good selectivity. NMO afforded the best selectivity and did not cause dissolution of the catalyst. The crystalline phase of the catalyst was found to have a fundamental role in controlling the activity of the catalyst, with maghemite NPs and wüstite powder showing no activity toward this oxidation reaction. Furthermore, smaller NPs were found to have a higher catalytic activity, which is easily understood because of their higher surface to volume ratio compared with that of larger NPs. The surface ligands had only a minor effect, with "bare" (hydroxylated surface) Fe_3O_4 NPs showing a higher initial conversion rate compared to that of stearate-capped Fe_3O_4 NPs, but with the same final reaction yield. This difference could be explained by activation of the catalyst by ligand detachment during the first catalytic cycle. It was demonstrated that Fe_3O_4 NPs could easily be recovered and recycled up to four times with minimal loss in activity. After multiple cycles, the spent catalyst lost its activity due to a phase change from magnetite to maghemite, but this change was reversible, and the previous catalyst activity could be fully recovered after one catalytic cycle at a high temperature. These results confirm that nonsupported magnetite nanocatalysts can be used as an affordable and recyclable catalyst for the selective MW-assisted oxidation of primary and secondary alcohols to aldehydes and ketones.

MATERIALS AND METHODS

Materials. Unless otherwise noted, commercially available materials were used without purification. The water content of the acetonitrile was determined with a Karl Fischer Moisture Titrator (MKC-610, Kyoto Electronics Company). Acetonitrile (MeCN) used as a solvent was found to contain 77 ppm of water. Superdry MeCN (10 ppm water) was tested but did not provide any improvement in yield for the standard oxidation reaction. Sodium stearate was purchased from Nacalai and $FeCl_3{\cdot}6H_2O$ from Wako.

Commercially available NPs were purchased from Sigma-Aldrich and Thermo Fisher: γ-Fe_2O_3 [nanopowder, <50 nm particle size (BET), Sigma-Aldrich], FeO (powder, −10 mesh, ≥99.6% trace metals basis, Sigma-Aldrich), and Fe_3O_4 [nanopowder, 50−100 nm particle size (SEM), 97% trace metal basis, Sigma-Aldrich].

Flash column chromatography was performed on Wakogel 60N, 38−100 μm, as described by Still et al.[68] or on a Biotage SP1 Flash Purification System with prepacked silica cartridges.

Instrumentation. ^{1}H and ^{13}C NMR spectra were recorded on a JEOL ECS-400NR NMR spectrometer (391.8 and 98.5 MHz, respectively). The ^{1}H chemical shift values are reported in parts per million (ppm, δ scale) and referenced to the ^{1}H resonance of $CDCl_3$ (δ 7.26). The NMR yield was determined for a crude product by ^{1}H NMR analysis by using 1,1,2,2-tetrachloroethane as an internal standard.

IR spectra were recorded on a PerkinElmer Spectrum One FT-IR spectrometer and reported in cm^{-1}. GC analysis was conducted with Shimadzu GC-2010 and GC-2010 Plus instruments equipped with a FID detector and a capillary column, ZB-1MS (Phenomenex Inc., 10 m × 0.10 mm i.d., 0.10 μm film thickness). High-resolution mass spectra were obtained using fast atom bombardment ionization or electron ionization on a JEOL JMS-700 mass spectrometer. Sample solutions were prepared by mixing an aliquot of the reaction mixture with methanol.

TEM was conducted with a JEM-1011 (JEOL) instrument at an accelerating voltage of 100 kV. The average diameter of the NPs was obtained from the analysis of more than 100 NPs with ImageJ software.[69]

UV−visible absorption spectra were acquired in a 1 cm quartz cuvette with a UV-2600 (Shimadzu) spectrometer. XRD patterns of the synthesized NPs were obtained on an X'Pert Pro MPD (PANalytical) instrument with Cu Kα radiation (λ = 1.542 Å) at 45 kV and 40 mA in the Bragg−Brentano configuration. XRD samples were prepared either by distributing the NP powder on a quartz substrate (used NPs) or by depositing the NP from the solution (pristine NPs), allowing for solvent evaporation in vacuo. XRD data were

https://doi.org/10.1021/acsomega.4c00361
ACS Omega 2024, 9, 24477−24488

collected in the range 2θ from 10° to 90° with a step of 0.1°. The size of the nanocrystals was estimated from the Debye−Scherrer equation applied to the half-width of peak corresponding to the Fe_3O_4 400 plane diffraction. The spectra were compared with the reference peaks of Fe_3O_4 (PDF 00-001-1111) and γ-Fe_2O_3 (PDF 00-25-1402).

Inductively coupled plasma atomic emission spectroscopy (ICP−AES) was performed on a Shimadzu ICPE-9800 system. Elemental analyses were carried out at the Microanalytical Laboratory of the Institute for Chemical Research, Kyoto University. Fe K-edge XANES spectra were acquired at BL14B2, SPring-8.

The amount of ligand on the NP surface was estimated by TG-DTA with a Shimadzu DTG-60. TG-DTA was performed by heating the sample to 873 K at a rate of 5 K/min and a flow rate of 50 mL/min of dry air.

MW reactions were performed using CEM Discover, equipped with 10 mL MW-resistant sealed tubes, and IR temperature control. Reactions under standard heating conditions were performed in sealed Schlenk tubes under constant stirring and heated by aluminum heaters (Chemstation).

Iron NP Synthesis. Monodispersed iron oxide NPs were synthesized by thermal decomposition of Fe(III) stearate according to a modified procedure reported by Hyeon and coworkers; see Scheme 2.[70]

Scheme 2. Synthesis of Stearate-Capped Fe_3O_4 NPs

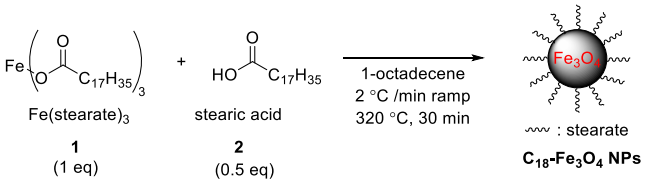

Iron(III) stearate was synthesized by ligand exchange from $FeCl_3{\cdot}6H_2O$ and sodium stearate in a mixture of water/ethanol/hexane 3:4:7 v/v kept at 70 °C for 4 h. To synthesize 13 nm Fe_3O_4 NPs, 5.76 g (6.4 mmol) of iron(III) stearate, 910 mg (3.2 mmol) of stearic acid, and 32 g of 1-octadecene were added to a two-neck round-bottom flask equipped with a temperature probe. The flask was deaerated three times by successive vacuum and an argon flow. The iron oxide NP synthesis was performed under a continuous argon flow. The flask was heated to 200 °C with a mantel heater, and then, the temperature was increased slowly (a heating rate of 3.3 °C per minute) to 320 °C, and the reaction mixture was kept at this temperature for 30 min. After slowly cooling to room temperature, the iron oxide NPs were purified by repeated washing in a methanol:hexane separatory funnel. The hexane layer containing the stearate-capped iron oxide NPs was then collected. The NPs were then further purified by three consecutive centrifugations in a mixture of hexane:acetone 5:9 v/v at 3500 rpm for 15 min. The NPs were then freeze-dried, and 0.53 g of powder was collected corresponding to an 85% yield (based on Fe atoms). The composition of the NPs was determined by elemental analysis (CHN microanalysis) and by ICP−AES for the iron content. For the ICP−AES analysis, the NPs were dissolved in a 5 wt % nitric acid by MW heating for 5 min at 80 °C.

Standard Microwave-Assisted Oxidation Reaction. To a 10 mL MW-transparent reaction vial, 0.8 mmol of 1-phenyl ethanol, 3.2 mg of stearate-capped iron oxide NPs (corresponding to 4 Fe mol % or equivalently 1.3 Fe_3O_4 mol % catalyst loading), 281 mg (2.4 mmol, 3 equiv) or 94 mg (0.8 mmol, 1 equiv) of NMO, and 0.8 mL of acetonitrile were added. The catalyst loading is typically expressed based on the molar concentration of iron species (all valencies included) instead of the molar concentration of the iron oxide species to allow for a better comparison between different iron catalysts. The sealed MW vial equipped with a special diaphragm cap for high-pressure reactions was introduced in the MW reactor and heated to 120 °C (38 °C above the boiling point of the solvent) for 15 h while continuously stirring. After completion, the reaction mixture was then left to cool to room temperature. A saturated aqueous solution of Na_2SO_3 was added until all remaining oxidant was quenched, and then extraction with water:ethyl acetate was repeated three times. The organic layers were combined, and the organic solvent was evaporated at a reduced pressure. A 0.8 mmol of 1,1,2,2-tetrachloroethane (internal standard) was added to the crude mixture, and a small aliquot of the crude mixture with internal standard was dissolved in $CDCl_3$ for ^1H NMR characterization, and the ^1H NMR spectrum was used to calculate the yield of the target compound.

Time-Course Study. For the time-course study, deuterated acetonitrile (MeCN-d_3) was used as solvent and 1,3,5-trimethoxybenzene was added prior to the reaction as an internal standard, and the yield was evaluated by taking a small aliquot of the reaction mixture with a gastight syringe at different time points making sure to avoid opening the sealed reaction vessel.

■ ASSOCIATED CONTENT

Supporting Information

The Supporting Information is available free of charge at https://pubs.acs.org/doi/10.1021/acsomega.4c00361.

Additional experimental details, materials, methods, and figures including XANES, FT-IR, TEM, TG-DTA, photographs of the pristine and spent catalyst, and magnetoseparation (PDF)

■ AUTHOR INFORMATION

Corresponding Authors

Francesca Pincella − *Institute for Chemical Research, Kyoto University, Uji, Kyoto 611-0011, Japan; Graduate School of Engineering, Kyoto University, Nishikyo-ku, Kyoto 615-8510, Japan;* orcid.org/0000-0001-8171-4272; Email: pincella@scl.kyoto-u.acjp

Katsuhiro Isozaki − *Institute for Chemical Research, Kyoto University, Uji, Kyoto 611-0011, Japan; Graduate School of Engineering, Kyoto University, Nishikyo-ku, Kyoto 615-8510, Japan;* orcid.org/0000-0002-0990-1708; Email: kisozaki@scl.kyoto-u.acjp

Hikaru Takaya − *Institute for Chemical Research, Kyoto University, Uji, Kyoto 611-0011, Japan; Graduate School of Engineering, Kyoto University, Nishikyo-ku, Kyoto 615-8510, Japan;* Present Address: Department of Life Science, Faculty of Life & Environmental Sciences, Teikyo University of Science, Tokyo 120−0045, Japan; Present Address: Institute for Molecular Science, Division of Photo-Molecular Science, Okazaki, Aichi 444−8585, Japan.; Email: takayahikaru@ntu.ac.jp

https://doi.org/10.1021/acsomega.4c00361
ACS Omega 2024, 9, 24477−24488

Masaharu Nakamura − *Institute for Chemical Research, Kyoto University, Uji, Kyoto 611-0011, Japan; Graduate School of Engineering, Kyoto University, Nishikyo-ku, Kyoto 615-8510, Japan;* orcid.org/0000-0002-1419-2117; Email: masaharu@scl.kyoto-u.acjp

Authors

Ryota Sato − *Institute for Chemical Research, Kyoto University, Uji, Kyoto 611-0011, Japan*

Toshiharu Teranishi − *Institute for Chemical Research, Kyoto University, Uji, Kyoto 611-0011, Japan;* orcid.org/0000-0002-5818-8865

Complete contact information is available at: https://pubs.acs.org/10.1021/acsomega.4c00361

Notes

The authors declare no competing financial interest.

■ ACKNOWLEDGMENTS

During this research, F.P. received the support of Japan Society for the Promotion of Science as an International Research Fellow of Japan Society for the Promotion of Science (Postdoctoral Fellowships for Research in Japan) and acknowledges the support from JSPS KAKENHI Grant Numbers 17F17759 and 16805188, the CREST program (11103784) of the Japan Science and Technology Agency (JST). XANES measurements were performed at Spring-8 on beamline BL14B2 with the approval of JASRI (2016B0121, 2017A0121). This work was supported by the FDRFP of Kyoto University Research Coordination Alliance. The authors thank Toshiko Hirano (ICR, Kyoto University) for performing the elemental analysis.

■ REFERENCES

(1) Dhakshinamoorthy, A.; Navalon, S.; Alvaro, M.; Garcia, H. Metal nanoparticles as heterogeneous Fenton catalysts. *ChemSusChem* **2012**, *5* (1), 46−64.

(2) Polshettiwar, V.; Luque, R.; Fihri, A.; Zhu, H.; Bouhrara, M.; Basset, J. M. Magnetically recoverable nanocatalysts. *Chem. Rev.* **2011**, *111* (5), 3036.

(3) Li, L.; Lv, J.; Shen, Y.; Guo, X.; Peng, L.; Xie, Z.; Ding, W. Hexadecylphosphate-Functionalized Iron Oxide Nanoparticles: Mild Oxidation of Benzyl C-H Bonds Exclusive to Carbonyls by Molecular Oxygen. *ACS Catal.* **2014**, *4* (8), 2746−2752.

(4) Yang, Q.; Fu, X.-P.; Jia, C.-J.; Ma, C.; Wang, X.; Zeng, J.; Si, R.; Zhang, Y.-W.; Yan, C.-H. Structural Determination of Catalytically Active Subnanometer Iron Oxide Clusters. *ACS Catal.* **2016**, *6* (5), 3072−3082.

(5) Moradi, L.; Sadeghi, S. H. Efficient pathway for the synthesis of amido alkyl derivatives using KCC-1/PMA immobilized on magnetic MnO2 nanowires as recyclable solid acid catalyst. *J. Mol. Struct.* **2023**, *1274*, 134477.

(6) Wang, Y.; Wang, R.; Lin, N.; Wang, Y.; Zhang, X. Highly efficient microwave-assisted Fenton degradation bisphenol A using iron oxide modified double perovskite intercalated montmorillonite composite nanomaterial as catalyst. *J. Colloid Interface Sci.* **2021**, *594*, 446−459.

(7) Sarveena, S.; Vargas, J. M.; Shukla, D. K.; Meneses, C. T.; Mendoza Zelis, P.; Singh, M.; Sharma, S. K. Synthesis, phase composition, Mossbauer and magnetic characterization of iron oxide nanoparticles. *Phys. Chem. Chem. Phys.* **2016**, *18* (14), 9561.

(8) Baeza, A.; Guillena, G.; Ramón, D. J. Magnetite and Metal-Impregnated Magnetite Catalysts in Organic Synthesis: A Very Old Concept with New Promising Perspectives. *ChemCatChem* **2016**, *8* (1), 49−67.

(9) Karimirad, F.; Behbahani, F. K. γ-Fe2O3@Si-(CH2)3@mel@(CH2)4SO3H as a magnetically bifunctional and retrievable nanocatalyst for green synthesis of benzo[c]acridine-8(9H)-ones and 2-amino-4H-chromenes. *Inorg. Nano-Met. Chem.* **2021**, *51* (5), 656−666.

(10) Sadri, Z.; Behbahani, F. K.; Keshmirizadeh, E. Synthesis and Characterization of a Novel and Reusable Adenine Based Acidic Nanomagnetic Catalyst and Its Application in the Preparation of 2-Substituted-2,3-dihydro −1H-perimidines under Ultrasonic Irradiation and Solvent-Free Condition. *Polycyclic Aromat. Compd.* **2023**, *43* (2), 1898−1913.

(11) Hasanzadeh, F.; Behbahani, F. K. Synthesis of 8-Aryl-7H-acenaphtho[1,2-d]imidazoles Using Fe3O4 NPs@GO@C4H8SO3H as a Green and Recyclable Magnetic Nanocatalyst. *Russ. J. Org. Chem.* **2020**, *56* (6), 1070−1076.

(12) Ferdousian, R.; Behbahani, F. K.; Mohtat, B. Synthesis and characterization of Fe(3)O(4)@Sal@Cu as a novel, efficient and heterogeneous catalyst and its application in the synthesis of 2-amino-4H-chromenes. *Mol. Diversity* **2022**, *26* (6), 3295−3307.

(13) Shokri, F.; Behbahani, F. K. Synthesis of Fe3O4@L-proline@SO3H as a novel and reusable acidic magnetic nanocatalyst and its application for the synthesis of N-substituted pyrroles at room temperature under ultrasonic irradiation and without solvent. *Inorg. Nano-Met. Chem.* **2022**, *52* (8), 1143−1152.

(14) Akbari, A.; Amini, M.; Tarassoli, A.; Eftekhari-Sis, B.; Ghasemian, N.; Jabbari, E. Transition metal oxide nanoparticles as efficient catalysts in oxidation reactions. *Nano-Struct. Nano-Objects* **2018**, *14*, 19−48.

(15) Doustkhah, E.; Mohtasham, H.; Hasani, M.; Ide, Y.; Rostamnia, S.; Tsunoji, N.; Hussein N Assadi, M. Merging periodic mesoporous organosilica (PMO) with mesoporous aluminosilica (Al/Si-PMO): A catalyst for green oxidation. *Mol. Catal.* **2020**, *482*, 110676.

(16) Doustkhah, E.; Rostamnia, S. Single site supported N -sulfonic acid and N -sulfamate onto SBA-15 for green and sustainable oxidation of sulfides. *Mater. Chem. Phys.* **2016**, *177*, 229−235.

(17) Rostamnia, S.; Alamgholiloo, H.; Jafari, M.; Rookhosh, R.; Abbasi, A. R. Synthesis and catalytic study of open metal site metal-organic frameworks of Cu3(BTC)2 microbelts in selective organic sulfide oxidation. *Appl. Organomet. Chem.* **2016**, *30* (11), 954−958.

(18) Wang, Y.; Arandiyan, H.; Liu, Y.; Liang, Y.; Peng, Y.; Bartlett, S.; Dai, H.; Rostamnia, S.; Li, J. Template-free Scalable Synthesis of Flower-like $Co_{3-x}Mn_xO_4$ Spinel Catalysts for Toluene Oxidation. *ChemCatChem* **2018**, *10* (16), 3429−3434.

(19) Najafishirtari, S.; Friedel Ortega, K.; Douthwaite, M.; Pattisson, S.; Hutchings, G. J.; Bondue, C. J.; Tschulik, K.; Waffel, D.; Peng, B.; Deitermann, M.; Busser, G. W.; Muhler, M.; Behrens, M. A Perspective on Heterogeneous Catalysts for the Selective Oxidation of Alcohols. *Chemistry* **2021**, *27* (68), 16809−16833.

(20) Mallat, T.; Baiker, A. Oxidation of Alcohols with Molecular Oxygen on Solid Catalysts. *Chem. Rev.* **2004**, *104*, 3037−3058.

(21) Mosallanejad, S.; Dlugogorski, B. Z.; Kennedy, E. M.; Stockenhuber, M. On the Chemistry of Iron Oxide Supported on gamma-Alumina and Silica Catalysts. *ACS Omega* **2018**, *3* (5), 5362−5374.

(22) Wang, Y.; Prinsen, P.; Mangin, F.; Yepez, A.; Pineda, A.; Rodríguez-Castellón, E.; Hasan Shah Gilani, M. R.; Xu, G.; Len, C.; Luque, R. Mechanistic insights into the microwave-assisted cinnamyl alcohol oxidation using supported iron and palladium catalysts. *Mol. Catal.* **2019**, *474*, 110409.

(23) Mittal, R.; Awasthi, S. K. A Synergistic Magnetically Retrievable Inorganic-Organic Hybrid Metal Oxide Catalyst for Scalable Selective Oxidation of Alcohols to Aldehydes and Ketones. *ChemCatChem* **2021**, *13* (22), 4799−4813.

(24) Rajabi, F.; Pineda, A.; Naserian, S.; Balu, A. M.; Luque, R.; Romero, A. A. Aqueous oxidation of alcohols catalysed by recoverable iron oxide nanoparticles supported on aluminosilicates. *Green Chem.* **2013**, *15* (5), 1232.

(25) Geng, L.; Zheng, B.; Wang, X.; Zhang, W.; Wu, S.; Jia, M.; Yan, W.; Liu, G. Fe3O4Nanoparticles Anchored on Carbon Serve the Dual

Role of Catalyst and Magnetically Recoverable Entity in the Aerobic Oxidation of Alcohols. *ChemCatChem* **2016**, *8* (4), 805−811.
(26) Zhang, S.; Zhao, X.; Niu, H.; Shi, Y.; Cai, Y.; Jiang, G. Superparamagnetic Fe3O4 nanoparticles as catalysts for the catalytic oxidation of phenolic and aniline compounds. *J. Hazard. Mater.* **2009**, *167* (1−3), 560.
(27) Zelmanov, G.; Semiat, R. Iron(3) oxide-based nanoparticles as catalysts in advanced organic aqueous oxidation. *Water Res.* **2008**, *42* (1−2), 492.
(28) Shaikh, M.; Satanami, M.; Ranganath, K. V. S. Efficient aerobic oxidation of alcohols using magnetically recoverable catalysts. *Catal. Commun.* **2014**, *54*, 91−93.
(29) Pereira, M. C.; Oliveira, L. C. A.; Murad, E. Iron oxide catalysts: Fenton and Fentonlike reactions - a review. *Clay Miner.* **2012**, *47* (3), 285−302.
(30) Shi, F.; Tse, M. K.; Pohl, M.-M.; Radnik, J.; Brückner, A.; Zhang, S.; Beller, M. Nano-iron oxide-catalyzed selective oxidations of alcohols and olefins with hydrogen peroxide. *J. Mol. Catal. A: Chem.* **2008**, *292* (1−2), 28−35.
(31) Sheldon, R. A. Recent advances in green catalytic oxidations of alcohols in aqueous media. *Catal. Today* **2015**, *247*, 4−13.
(32) Huang, H.-H.; Lu, M.-C.; Chen, J.-N. Catalytic Decomposition of Hydrogen Peroxide and 2-chlorophenol with iron oxides. *Water Res.* **2001**, *35* (9), 2291−2299.
(33) Shi, F.; Tse, M. K.; Pohl, M. M.; Bruckner, A.; Zhang, S.; Beller, M. Tuning catalytic activity between homogeneous and heterogeneous catalysis: improved activity and selectivity of free nano-Fe2O3 in selective oxidations. *Angew. Chem., Int. Ed. Engl.* **2007**, *46* (46), 8866.
(34) Pillai, U. Oxidation of alcohols over Fe3+/montmorillonite-K10 using hydrogen peroxide. *Appl. Catal., A* **2003**, *245* (1), 103−109.
(35) Liu, G.; Huang, H.; Xie, R.; Feng, Q.; Fang, R.; Shu, Y.; Zhan, Y.; Ye, X.; Zhong, C. Enhanced degradation of gaseous benzene by a Fenton reaction. *RSC Adv.* **2017**, *7* (1), 71−76.
(36) Navalon, S.; Dhakshinamoorthy, A.; Alvaro, M.; Garcia, H. Heterogeneous fenton catalysts based on activated carbon and related materials. *ChemSusChem* **2011**, *4* (12), 1712.
(37) Thomas, N.; Dionysiou, D. D.; Pillai, S. C. Heterogeneous Fenton catalysts: A review of recent advances. *J. Hazard. Mater.* **2021**, *404* (Pt B), 124082.
(38) Martínez, F.; Calleja, G.; Melero, J. A.; Molina, R. Heterogeneous photo-Fenton degradation of phenolic aqueous solutions over iron-containing SBA-15 catalyst. *Appl. Catal., B* **2005**, *60* (3−4), 181−190.
(39) Pliego, G.; Zazo, J. A.; Casas, J. A.; Rodriguez, J. J. Case study of the application of Fenton process to highly polluted wastewater from power plant. *J. Hazard. Mater.* **2013**, *252*−*253*, 180.
(40) Xu, P.; Zeng, G. M.; Huang, D. L.; Feng, C. L.; Hu, S.; Zhao, M. H.; Lai, C.; Wei, Z.; Huang, C.; Xie, G. X.; Liu, Z. F. Use of iron oxide nanomaterials in wastewater treatment: a review. *Sci. Total Environ.* **2012**, *424*, 1−10.
(41) Neumann, R. *Modern Oxidation Methods*. Wiley VCH: Germany, 2010.
(42) Vijayasri, K.; Rajaram, J.; Kuriacose, J. C. Ruthenium(III)-catalysed oxidation of secondary alcohols by N-methylmorpholine N-oxide (NMO). *J. Mol. Catal.* **1987**, *39* (2), 203−217.
(43) Griffith, W. P.; Jolliffe, J. M.; Ley, S. V.; Springhorn, K. F.; Tiffin, P. D. Oxidation of Activated Halides to Aldehydes and Ketones by N-Methylmorpholine-N-oxide. *Synth. Commun.* **1992**, *22* (13), 1967−1971.
(44) Khumraksa, B.; Phakhodee, W.; Pattarawarapan, M. Rapid oxidation of organic halides with N-methylmorpholine N-oxide in an ionic liquid under microwave irradiation. *Tetrahedron Lett.* **2013**, *54* (15), 1983−1986.
(45) Moore, P. W.; Read, C. D. G.; Bernhardt, P. V.; Williams, C. M. ATP3 and MTP3: Easily Prepared Stable Perruthenate Salts for Oxidation Applications in Synthesis. *Chemistry* **2018**, *24* (18), 4556−4561.
(46) Ley, S.; Norman, J.; Griffith, W. P.; Marsden, S. P. Tetrapropylammonium Perruthenate, Pr4N+RuO4-TPAP: A Catalytic Oxidant for Organic Synthesis. *Synthesis* **1994**, *1994* (07), 639−666.
(47) Rosenau, T.; French, A. D. N-Methylmorpholine-N-oxide (NMMO): hazards in practice and pitfalls in theory. *Cellulose* **2021**, *28* (10), 5985−5990.
(48) Swaddle, T. W.; Oltmann, P. Kinetics of the magnetite-maghemite-hematite transformation, with special reference to hydrothermal systems. *Can. J. Chem.* **1980**, *58* (17), 1763−1772.
(49) Liu, J.; Wu, Z.; Tian, Q.; Wu, W.; Xiao, X. Shape-controlled iron oxide nanocrystals: synthesis, magnetic properties and energy conversion applications. *CrystEngComm* **2016**, *18* (34), 6303−6326.
(50) Schwaminger, S. P.; Bauer, D.; Fraga-García, P.; Wagner, F. E.; Berensmeier, S. Oxidation of magnetite nanoparticles: impact on surface and crystal properties. *CrystEngComm* **2017**, *19* (2), 246−255.
(51) Nie, S.; Starodub, E.; Monti, M.; Siegel, D. A.; Vergara, L.; El Gabaly, F.; Bartelt, N. C.; de la Figuera, J.; McCarty, K. F. Insight into magnetite's redox catalysis from observing surface morphology during oxidation. *J. Am. Chem. Soc.* **2013**, *135* (27), 10091.
(52) Okudera, H.; Yoshiasa, A.; Murai, K.-i.; Okube, M.; Takeda, T.; Kikkawa, S. Local structure of magnetite and maghemite and chemical shift in Fe K-edge XANES. *J. Mineral. Petrol. Sci.* **2012**, *107* (3), 127−132.
(53) Feld, A.; Weimer, A.; Kornowski, A.; Winckelmans, N.; Merkl, J. P.; Kloust, H.; Zierold, R.; Schmidtke, C.; Schotten, T.; Riedner, M.; Bals, S.; Weller, H. Chemistry of Shape-Controlled Iron Oxide Nanocrystal Formation. *ACS Nano* **2019**, *13* (1), 152−162.
(54) Cornell, R. M.; Schwertmann, U. *The Iron Oxides: Structure, Properties, Reactions, Occurrences*; Wiley VCH, 2006.
(55) Radu, T.; Iacovita, C.; Benea, D.; Turcu, R. X-Ray Photoelectron Spectroscopic Characterization of Iron Oxide Nanoparticles. *Appl. Surf. Sci.* **2017**, *405*, 337−343.
(56) Ruan, H. D.; Frost, R. L.; Kloprogge, J. T.; Duong, L. Infrared spectroscopy of goethite dehydroxylation: III. FT-IR microscopy of in situ study of the thermal transformation of goethite to hematite. *Spectrochim. Acta, Part A* **2002**, *58* (5), 967.
(57) Ruan, H. D.; Frost, R. L.; Kloprogge, J. T.; Duong, L. Infrared spectroscopy of goethite dehydroxylation. II. Effect of aluminium substitution on the behaviour of hydroxyl units. *Spectrochim. Acta, Part A* **2002**, *58*, 479−491.
(58) Ruan, H. D.; Frost, R. L.; Kloprogge, J. T. The behavior of hydroxyl units of synthetic goethite and its dehydroxylated product hematite. *Spectrochim. Acta, Part A* **2001**, *57*, 2575−2586.
(59) Poling, G. W. Infrared Reflection Studies of the Oxidation of Copper and Iron. *J. Electrochem. Soc.* **1969**, *116* (7), 958−963.
(60) Namduri, H.; Nasrazadani, S. Quantitative analysis of iron oxides using Fourier transform infrared spectrophotometry. *Corros. Sci.* **2008**, *50* (9), 2493−2497.
(61) Nasrazadani, S.; Raman, A. The application of infrared spectroscopy to the study of rust systems—II. Study of cation deficiency in magnetite (Fe_3O_4) produced during its transformation to maghemite (γ-Fe_2O_3) and hematite (α-Fe_2O_3). *Corros. Sci.* **1993**, *34* (8), 1355−1365.
(62) Fujimori, A.; Ohmura, K.; Honda, N.; Kakizaki, K. Creation of high-density and low-defect single-layer film of magnetic nanoparticles by the method of interfacial molecular films. *Langmuir* **2015**, *31* (10), 3254.
(63) Wang, N.; Wang, P. Study and application status of microwave in organic wastewater treatment - A review. *Chem. Eng. J.* **2016**, *283*, 193−214.
(64) Crosswhite, M.; Hunt, J.; Southworth, T.; Serniak, K.; Ferrari, A.; Stiegman, A. E. Development of Magnetic Nanoparticles as Microwave-Specific Catalysts for the Rapid, Low-Temperature Synthesis of Formalin Solutions. *ACS Catal.* **2013**, *3* (6), 1318−1323.
(65) Seki, T.; Chiang, K. Y.; Yu, C. C.; Yu, X.; Okuno, M.; Hunger, J.; Nagata, Y.; Bonn, M. The Bending Mode of Water: A Powerful Probe for Hydrogen Bond Structure of Aqueous Systems. *J. Phys. Chem. Lett.* **2020**, *11* (19), 8459−8469.

https://doi.org/10.1021/acsomega.4c00361
ACS Omega 2024, 9, 24477−24488

(66) Rosenau, T.; Potthast, A.; Kosma, P.; Chen, C.-L.; Gratzl, J. S. Autocatalytic Decomposition of N-Methylmorpholine N-Oxide Induced by Mannich Intermediates. *J. Org. Chem.* **1999**, *64*, 2166−2167.
(67) Bur, S. K. 6.17 Polonovski- and Pummerer-type Reactions and the Nef Reaction. In *Comprehensive Organic Synthesis II*; Elsevier, 2014; pp 755−801..
(68) Still, W. C.; Kahn, M.; Mitra, A. Rapid chromatographic technique for preparative separations with moderate resolution. *J. Org. Chem.* **1978**, *43* (14), 2923−2925.
(69) Schneider, C. A.; Rasband, W. S.; Eliceiri, K. W. NIH Image to ImageJ: 25 years of image analysis. *Nat. Methods* **2012**, *9* (7), 671.
(70) Park, J.; An, K.; Hwang, Y.; Park, J. G.; Noh, H. J.; Kim, J. Y.; Park, J. H.; Hwang, N. M.; Hyeon, T. Ultra-large-scale syntheses of monodisperse nanocrystals. *Nat. Mater.* **2004**, *3* (12), 891.

https://doi.org/10.1021/acsomega.4c00361
ACS Omega 2024, 9, 24477−24488